

Effects of the Rotation Phase on the Average Lift of an Insect-Like Flapping Wing

Vu Dan Thanh Le¹, Anh Tuan Nguyen^{1*}, Thanh Dong Pham¹,
Hoang Quan Dinh¹, Huu The Nguyen¹, Cong Truong Dinh²

¹Le Quy Don Technical University, Ha Noi, Vietnam

²Hanoi University of Science and Technology, Ha Noi, Vietnam

*Corresponding author email: atnguyen@lqdtu.edu.vn

Abstract

Insect-like flapping wings are characterized by multi-degree-of-freedom motions at the wing base, which can be divided into two main movements: sweep and rotation. The phase difference between sweep and rotation motions is an important kinematic parameter that has a great influence on the wing lift. In this paper, the effect of the rotation phase on the average lift of a hawkmoth-like wing is investigated. Simulations were conducted using a Fluid-Structure Interaction co-simulation framework developed based on the multibody dynamics approach and an unsteady vortex-lattice method. The results show that maximum lift for the rigid wing is reached at an advanced phase of about 10%. For the flexible wing, maximum lift is reached at a delayed phase of about 5%. The reason for this difference could be the passive deformation of the flexible wing, which causes an advanced rotation phase at the wing tip. The obtained results are in good agreement with experimental results conducted by previous studies.

Keywords: Flapping wing, micro air vehicles, unsteady aerodynamics.

1. Introduction

Insect-like Flapping Wing Micro Air Vehicles (FWMAVs) have many advantages over conventional flight vehicles, especially at low-speed ranges. They can be used for reconnaissance, military technology, emergency rescue inside confined spaces, etc [1-3]. These micro air vehicles are often designed to mimic insects in nature, with complicated flapping mechanisms characterized by high flapping frequency and multi-degree-of-freedom motion at the wing base [4]. The aerodynamic unsteadiness is therefore significant [5].

Each flapping cycle of insects can be divided into two phases: upstroke and downstroke (Fig. 1 [7]). The wing motion can be divided into two main movements, corresponding to two Euler angles: the sweep angle ϕ for sweeping motion, and the rotation angle α for rotational motion. During a cycle, the wings beat roughly in a stroke plane, which is defined by the wing base and the wing tip of the maximum and minimum sweep positions (Points P_1 and P_2 in Fig. 1). The y_0 axis of the stroke-plane fixed coordinate system ($x_0 y_0 z_0$) is parallel to the horizontal direction, z_0 is perpendicular to the stroke plane [6]. The sweep angle ϕ is defined as the angle formed by the y_0 axis and wing axis y_w . The rotation angle α is defined as the angle between the wing chord and the stroke plane.

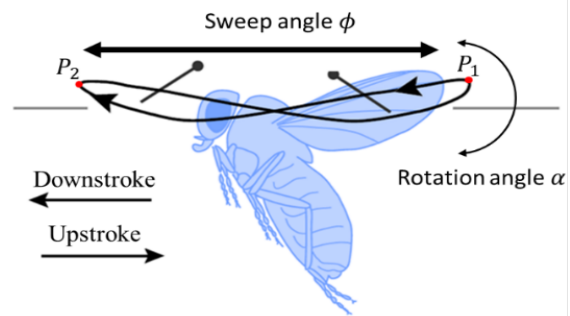


Fig. 1. Flapping mechanism of insects wing

At the end of each stroke, the wing performs a quick rotation along the wingspan to flip the wing in the opposite direction. The phase difference between rotation and sweeping motion is called the rotation phase. If the wing flips ($\alpha = 90^\circ$) before it changes the direction (the angle ϕ takes its maximum or minimum value at P_1 or P_2 points), it is called the advanced rotation phase and vice versa.

Many studies have shown that the rotation phase is an important kinematic parameter that has a great influence on the wing lift. Dickinson's experiment on the *Drosophila* fruit fly [8] showed that the delayed phase is not beneficial for generating lift.

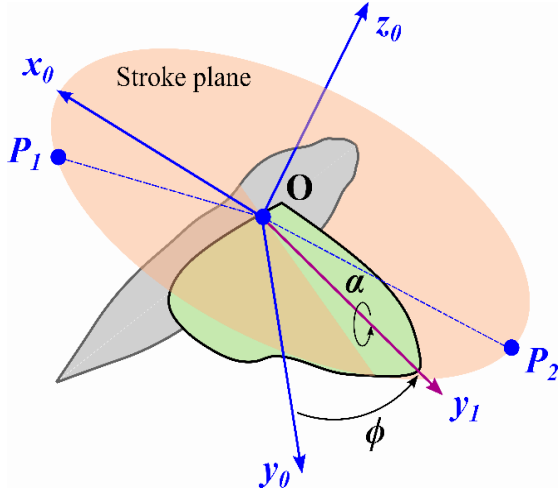


Fig. 2. Definition of Euler angles

In general, researchers agree that an advanced phase would be beneficial in terms of lift [9-11] as well as aerodynamic quality [12]. According to Lua *et al.* [12], in the advanced phase case, when the wing changes its sweep direction, the positive pitch angle combined with the induced velocity of the vortex from the previous stroke could increase lift.

Previous studies have mainly focused on rigid wings. Insect wings are flexible membrane structures, reinforced with veins. The wings of insect-like FWMAVs are made of lightweight materials to ensure take-off mass and engine performance. With such structures, the deformation of the wings under aerodynamic and inertial loads on the flight is unavoidable. In this paper, an Fluid - Structure Interaction (FSI) co-simulation framework is deployed to determine the lift of a hawkmoth-like wing in hovering flight. Simulations are conducted with different values of the rotation phase for both rigid and flexible wings, thereby evaluating its influence on the lift force.

2. Methodology

The FSI co-simulation framework used in this paper is a coupling of an aerodynamics solver based on the Unsteady vortex lattice method (UVLM) and a dynamics solver based on the multibody-dynamics (MBD) approach. The model has been presented thoroughly in [6] and will be presented briefly in this section to ensure the consistency of the paper.

2.1. Aerodynamic Model

In the UVLM aerodynamics solver, insect wings are considered to be very thin and discretized into N panels, on each a vortex ring consisting of four straight bound-vortex segments with equal circulation is applied [13]. Each panel has a collocation point at its centroid. When the air flows around the wing, a wake is shed from the trailing edge and freely moves with the particles of the air stream (Fig. 3).

The non-penetration boundary condition must be satisfied at all collocation points on the wing surface, i.e. the normal component of the relative velocity is zero:

$$[\mathbf{V}_\infty + \mathbf{V}_{ib}(\mathbf{r}, t) + \mathbf{V}_{iw}(\mathbf{r}, t) - \mathbf{V}_w(\mathbf{r}, t)] \cdot \mathbf{n} = 0, \quad (1)$$

where \mathbf{V}_∞ is the freestream velocity; \mathbf{V}_{ib} and \mathbf{V}_{iw} denote the velocities due to bound-vortex segments on the wing and the free wake, respectively; \mathbf{V}_w is the velocity of the wing; \mathbf{n} is the local normal vector of the wing surface.

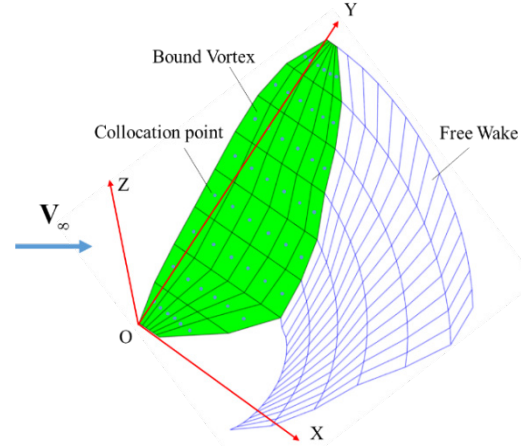


Fig. 3. UVLM aerodynamic model

The induced velocities caused by each vortex segment were determined according to the Biot-Savart formula. Equation (1) can be rewritten for the k^{th} collocation point as:

$$\sum_{i=1}^N a_i^k \Gamma_i = -[\mathbf{V}_\infty + \mathbf{V}_{iw}^k(\mathbf{r}, t) - \mathbf{V}_w^k(\mathbf{r}, t)] \cdot \mathbf{n}^k, \quad (2)$$

where upper index k denotes the quantity determined at the k^{th} collocation point, Γ_i is the circulation of vortex segments in the i^{th} panel, a_i^k is the normal component of the induced velocity at the k^{th} collocation point, caused by the i^{th} vortex on the wing surface if the circulation is assumed to equal 1. Thus, a corresponding system of N equations are derived for N collocation points, which can be written in matrix form as follows:

$$\begin{bmatrix} a_1^1 & a_2^1 & \cdots & a_N^1 \\ a_1^2 & a_2^2 & \cdots & a_N^2 \\ \vdots & \vdots & \ddots & \vdots \\ a_1^N & a_2^N & \cdots & a_N^N \end{bmatrix} \times \begin{bmatrix} \Gamma_1 \\ \Gamma_2 \\ \vdots \\ \Gamma_N \end{bmatrix} = \begin{bmatrix} RHS_1 \\ RHS_2 \\ \vdots \\ RHS_N \end{bmatrix} \quad (3)$$

where RHS_k denotes the right-hand side of equation (2) for the k^{th} collocation point. The circulation of each vortex segment Γ_i is determined after solving (3). Then, the pressure distribution on the surface can be determined according to the unsteady Bernoulli equation [13].

2.2. FSI Co-Simulation Framework

The aerodynamic load distributed on the wing surface is converted into the form of external

concentrated forces and moments for the MBD solver. The wing structure is modeled by N_b rigid bodies connected with bending and torsion springs (Fig. 4).

The generalized coordinate vector used to determine the state of the MBD system is $\Phi = [\theta_2, \alpha_2, \theta_3, \alpha_3, \dots, \theta_{N_b}, \alpha_{N_b}]^T$, where θ_k and α_k denote the bending and torsion angles of the corresponding springs.

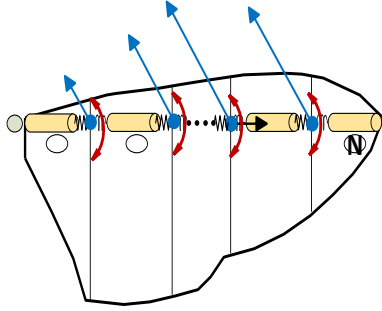


Fig. 4. Spring-bodies system

Using the Lagrangian method, the equations of motion of the MBD system can be written in the matrix form as follows:

$$M(\Phi, \dot{\Phi}, t)\ddot{\Phi} + H(\Phi, \dot{\Phi}, t) = Q(\Phi, \dot{\Phi}, t), \quad (4)$$

where M , H , Q are the generalized mass matrix, generalized stiffness matrix, and generalized force matrix, respectively.

Using the Lagrangian method, the equations of motion of the MBD system can be written in the matrix form as follows: A two-way FSI coupling strategy is employed for information exchange between the dynamic and aerodynamic models (Fig. 5).

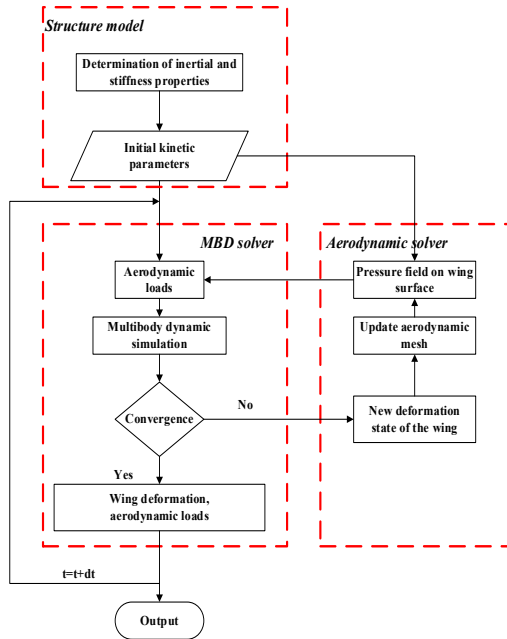


Fig. 5. FSI co-simulation framework

At each iteration, the new location of the nodes on the aerodynamic mesh is interpolated using the wing deformation from the MBD solver, and therefore to determine the aerodynamic load. The MBD solver is then used to determine the new deformation state of the wing after converting the aerodynamic load from the aerodynamic solver to point forces and torques. For solving the system of nonlinear differential equations, a quasi-Newtonian method based on the line-search theory is employed [14].

2.3. Validation

First, the multibody dynamics model is validated by a simplified system with three bodies connected by bending and torsion springs as shown in Fig. 6.

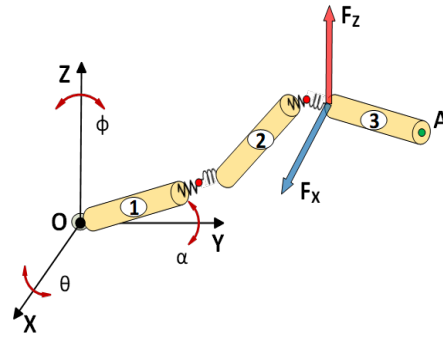


Fig. 6. Multibody system for validation

Table 1. Parameters of the bodies

Parameters	Body 1	Body 2	Body 3
Length (cm)	1.61	1.61	1.61
Mass (mg)	13.27	13.01	7.48
Inertia moment ($kg \cdot m^2$)	0.47×10^{-10}	3.84×10^{-10}	1.26×10^{-10}

The parameters of the bodies are shown in Table 1.

The motion of the spherical joint at the system origin is determined by three Euler angles as follows:

$$\begin{aligned} \phi(t) &= \frac{\pi}{3} \cos(2\pi ft) \\ \alpha(t) &= -\frac{\pi}{3} \sin(2\pi ft) \\ \theta(t) &= \frac{10}{180} \pi \cos(4\pi ft), \end{aligned} \quad (5)$$

where flapping frequency f is 26 Hz.

At the joint between the second and third bodies, forces are applied in the X and Z directions:

$$\begin{aligned} F_x(t) &= 0,02 \sin(2\pi ft) \text{ (N)} \\ F_z(t) &= 0,04 \cos(2\pi ft) \text{ (N)} \end{aligned} \quad (6)$$

The simulation results are compared with a similar model built in the commercial software MSC/ADAMS. The comparison of the simulation results for the coordinates along the axes of point A at the tip of the third body is shown in Fig. 7.

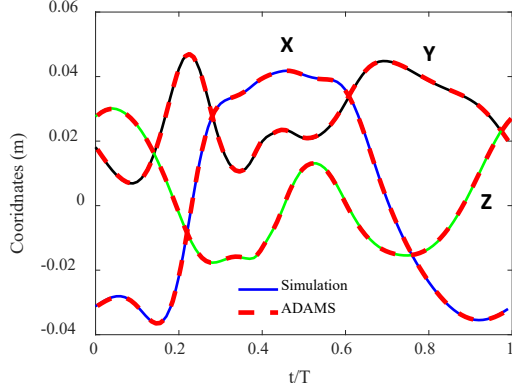


Fig. 7. Compare the coordinates of point A along the axes

The results of the two methods are completely consistent with each other. This confirms the accuracy of the multibody dynamic model.

Then, the proposed FSI model is validated by comparing the simulated lift coefficient of an insect wing model with the experimental results obtained by Lua *et al.* [15]. In that experiment, a hawkmoth-like wing model underwent harmonic motions similar to those of hovering insects. The corresponding Euler angle functions are:

$$\begin{aligned}\phi(t) &= \frac{\pi}{3} \cos(2\pi ft) \\ \alpha(t) &= -\frac{\pi}{3} \sin(2\pi ft)\end{aligned}\quad (7)$$

The experiment was performed at a Reynolds number of 6000. The simulated lift coefficient in a flapping period is shown in Fig. 8 [15].

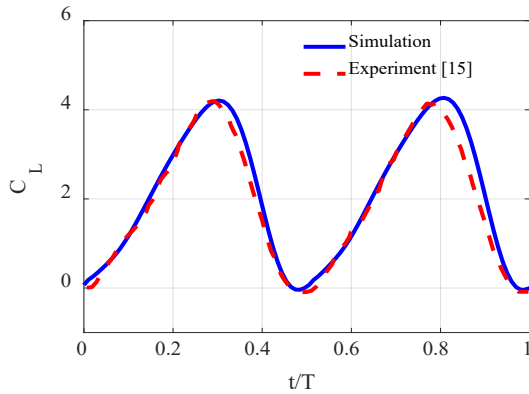


Fig. 8. Comparison of the lift coefficient with the experiment

It can be seen that the results obtained from the simulation are quite similar to the experimental data. The average simulated lift coefficient in a flapping period is 2.06, which is close to the experimental value of 2.08 with an error of 1.17%. This proves the accuracy of the proposed model.

3. Simulation Results

The present framework is used to study a wing model based on the hawkmoth *Manduca Sexta* wing. The wing structure model is built based on the experimental data of O'Hara and Palazotto [16]. Details of this process can be found in [6]. Some geometric and inertial parameters of the wing model are shown in Table 2.

Table 2. Wing parameters

Parameters	Unit	Values
Wing mass	mg	43.4
Wing area	mm ²	815.3
Wing length	mm	48.3
Mean chord	mm	18.4

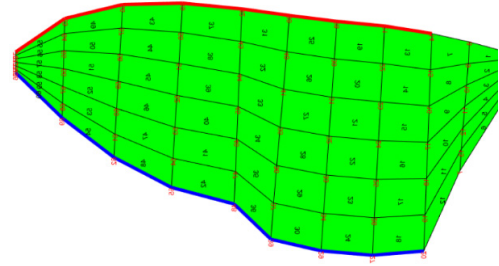


Fig. 9. Aerodynamic mesh

The aerodynamic mesh in the UVLM solver is shown in Fig. 9. A mesh resolution of 6×10 (6 chordwise and 10 spanwise panels) is chosen as recommended by [17].

The motion at the wing base is represented by periodic functions based on experimental data by Willmott and Ellington [18] for hovering hawkmoths:

$$\begin{aligned}\phi(t) &= 10^\circ + 50^\circ \cos(2\pi(ft + \delta\psi)) \\ \alpha(t) &= 90^\circ - 45^\circ \sin(2\pi ft),\end{aligned}\quad (8)$$

with a flapping frequency f equals 26.1 Hz.

In (8), $\delta\psi$ is the rotation phase, expressed as a fraction of the flapping period. $\delta\psi$ is negative in an advanced phase case, and positive in a delayed phase.

In this paper, a parameter analysis of $\delta\psi$ was conducted, taking values from -20% to 10% for the rigid wing, and from -10% to 10% for the flexible wing. For each case, we determined the lift force L and the average lift in a flapping cycle L^m .

Fig. 10 shows the variation of Euler angles in one flapping period for different cases: advanced phase, symmetrical, and delayed phase. The downstroke starts when the sweep angle ϕ reaches its maximum value. The wing rotates to change direction when the rotation angle $\alpha = 90^\circ$ (point A in Fig. 10). The rotation phase $\delta\psi$ is defined by the distance from this point to the beginning of the flapping cycle.

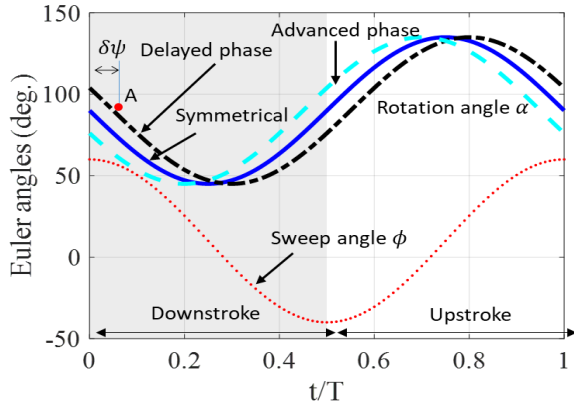


Fig. 10. Variation of Euler angles in one flapping period.

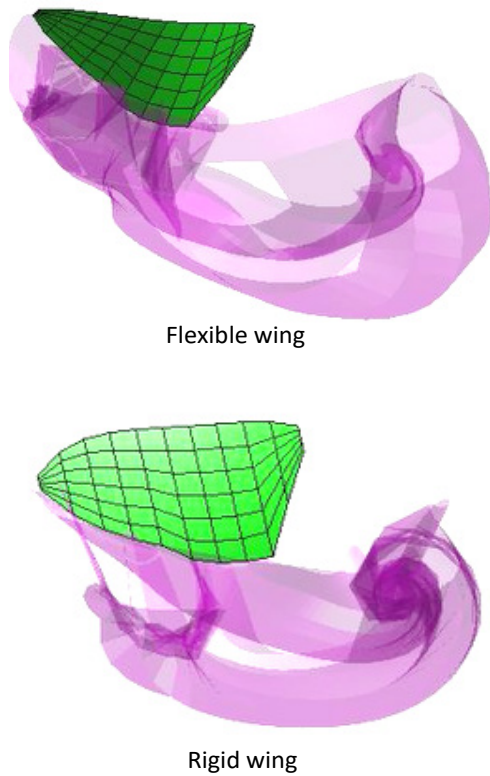


Fig. 11. Wake visualization of the flexible and rigid wings

Fig. 11 shows the wing state and wake visualization of the flexible and rigid wings obtained by the present program.

Fig. 12a shows the average lift in one flapping period with different values of the rotation phase for the rigid wing. The maximum average lift is achieved at an advanced phase of 10% ($\delta\psi = -10\%$), similar to the results obtained from previous studies [12]. The average lift decreases rapidly as the rotation phase increases. When the phase is too advanced ($\delta\psi < -10\%$), the average lift also decreases.

To explain the variation trend of the average lift for the rigid wing, Fig. 12b shows the lift force in a flapping period for three cases: $\delta\psi = -15\%$, $\delta\psi = -10\%$, and $\delta\psi = 5\%$. When $\delta\psi = -10\%$, there is a significant increase in lift at the beginning of each stroke. With this value of the rotation phase, the wing takes advantage of the induced velocity of the wake from the previous flapping cycle. At the midpoint of each stroke, the wing's translational velocity and also the aerodynamic force reach maximum values. In the case of the advanced phase, this moment coincides with a pitch-up movement of the wing, which increases lift. When the rotation phase is delayed ($\delta\psi = 5\%$), there is a significant decrease in lift at the midpoint of each stroke.

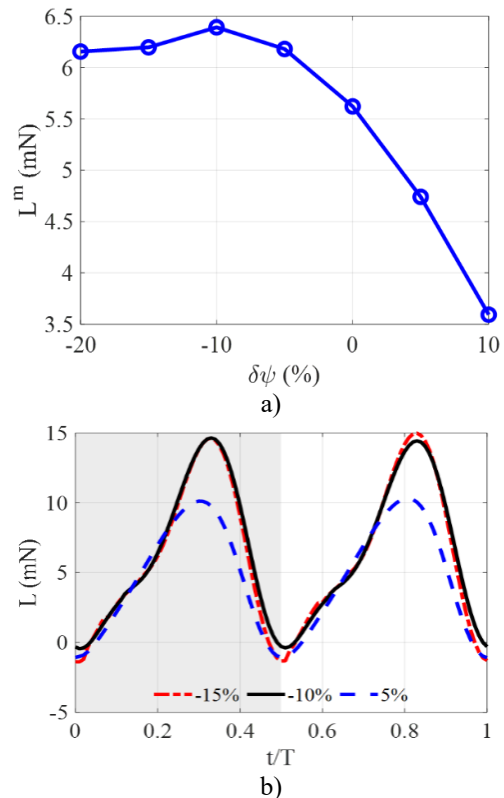


Fig. 12. Effect of rotation phase on the lift force of the rigid wing: a) Average lift versus rotation phase, b) Comparison of lift in a flapping period with different rotation phases

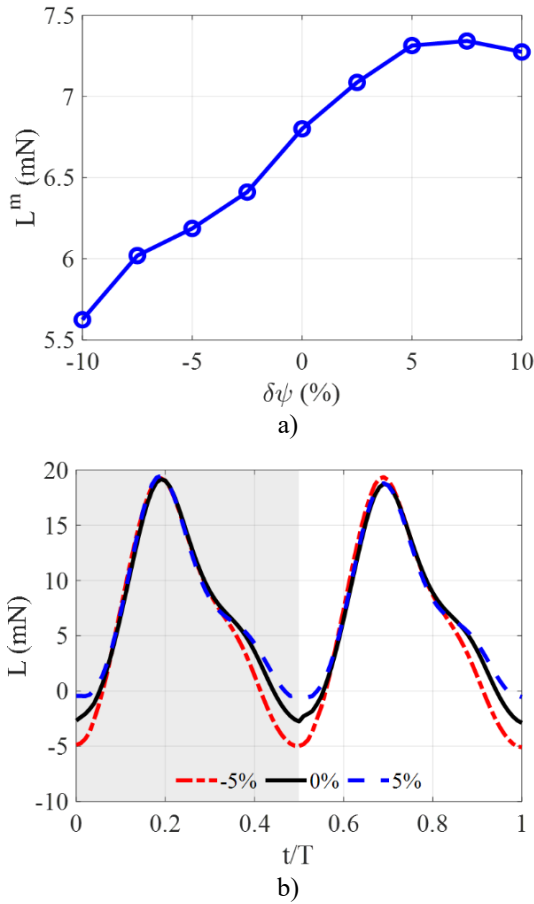


Fig. 13. Effect of rotation phase on the lift force of the flexible wing: a) Average lift versus rotation phase, b) Comparison of lift in a flapping period with different rotation phases

The influence of the rotation phase on the mean lift of the flexible wing is shown in Fig. 13a. The variation trend of the flexible wings is opposite to that of the rigid counterpart. The maximum average lift is achieved at a delayed phase of about 7%. The average lift decreases sharply as $\delta\psi$ declines. A comparison of lift in a flapping cycle for different rotation phases in Fig. 13b shows that lift differs mainly at the beginning of each stroke. Lift force increases as $\delta\psi$ grows.

To explain the contradiction between the results for rigid and flexible wings, the following section will investigate the effect of the structure deformation on the rotation phase in the wing base and the wing tip of the flexible wing. Fig. 14 shows the variation of Euler angles during a flapping period at the wing base and the wing tip. Subscripts b and t denote the Euler angles at the wing base and wing tip, respectively. It can be seen that due to wing deformation, at the wing tip, the phase of sweeping motion is delayed while that of rotation motion is advanced.

Fig. 15 shows the phase difference between the wing rotations at the wing tip and wing base. It is observed that when the rotation phase is delayed by

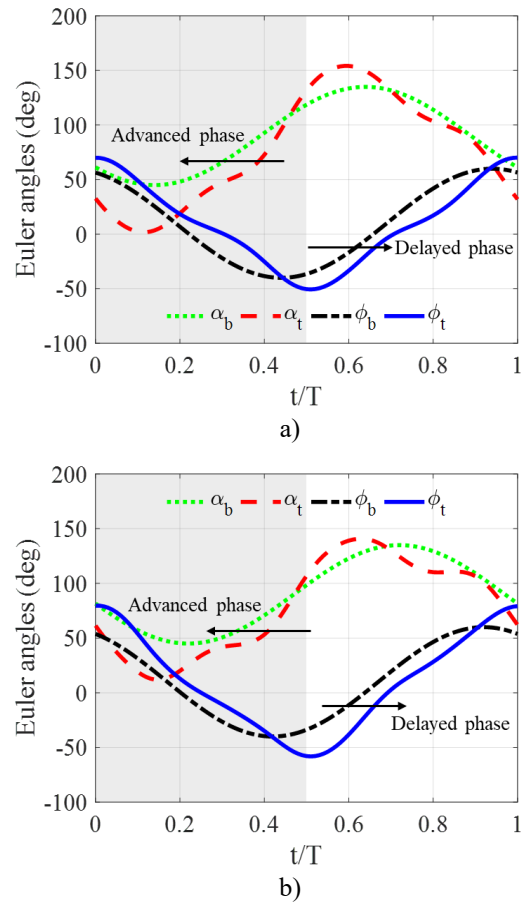


Fig. 14. Variation of the Euler angles in a flapping period: a) $\delta\psi = -5\%$, b) $\delta\psi = 5\%$

10% at the wing base, that at the wing tip is advanced by 3%. Therefore, a large lift is generated in this case. Similarly, when the rotation phase is advanced by 10% at the wing base, the rotation phase at the wing tip is advanced by 15%, which leads to a significant reduction in lift.

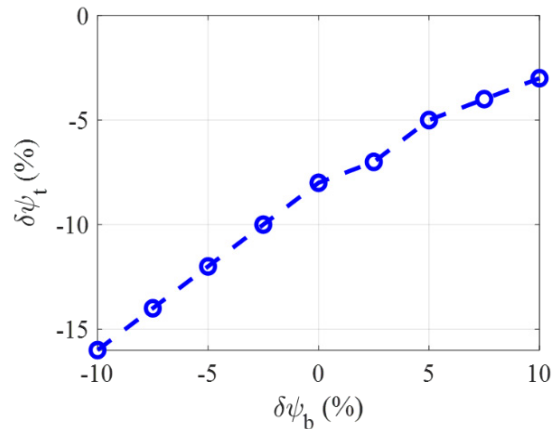


Fig. 15. Comparison of the phase difference between wing tip and wing base

These above results have confirmed the conclusion of some previous studies that the advanced rotation phase could increase lift for rigid wings. However, for flexible wings, due to the phase difference between the wing base and wing tip under the effect of deformation, phase advance at the wing base could lead to a significant decrease in lift. Maximum lift of the flexible wing is reached at a phase delay of 5% at the wing base. Therefore, in the designing process of wing motion for FWMAV with flexible wings, the phase difference between the wing base and the wing tip due to the deformation must be considered.

4. Conclusion

This paper studies the effect of the rotation phase on the lift force of insect-like FWMAV. The simulation is conducted using a FSI co-simulation framework based on the UVLM aerodynamics solver and the MBD approach. The results show that phase advance is beneficial in terms of lift for rigid wings. However, for flexible wings, there is a phase difference between the motions at the wing tip and wing base due to structure deformation. The maximum lift of the flexible wing is obtained when the rotation phase at the wing base is delayed by about 5%.

Thus, when designing the law of wing motion for insect-like FWMAV, it is necessary to pay attention to this phase difference.

Acknowledgments

This research is funded by Vietnam National Foundation for Science and Technology Development (NAFOSTED) under grant number 107.01-2021.39.

References

- [1] H. V. Phan, S. Aurecianus, T. Kang, and H. C. Park, KUBeetle-S: An insect-like, tailless, hover-capable robot that can fly with a low-torque control mechanism, *International Journal of Micro Air Vehicles*, Oct. 15, 2019. <https://doi.org/10.1177/1756829319861371>
- [2] M. Perçin, G.C.H.E. de Croon, B.D.W. Remes, R. Ruijsink, C. De Wagter, *The DelFly: Design, Aerodynamics, and Artificial Intelligence of a Flapping Wing Robot*, Springer, 2016. <https://doi.org/10.1007/978-94-017-9208-0>
- [3] N. T. Jafferis, E. F. Helbling, M. Karpelson, and R. J. Wood, Untethered flight of an insect-sized flapping-wing microscale aerial vehicle, *Nature* 570, pp. 491-495, Jun. 2019. <https://doi.org/10.1038/s41586-019-1322-0>
- [4] A. T. Nguyen, T. D. Pham, C. T. Dinh, and J. H. Han, An integrated program to simulate the multibody dynamics of flapping flight, *JST: Smart Systems and Devices*, vol. 31, iss. 1, pp. 76-83, May. 2021. <https://doi.org/10.51316/jst.150.ssad.2021.31.1.10>
- [5] B. Cheng, J. Roll, Y. Liu, D. R. Troolin, and X. Deng, Three-dimensional vortex wake structure of flapping wings in hovering flight, *Journal of The Royal Society Interface*, vol. 11, iss. 91, Feb. 2014, pp. 20130984. <https://doi.org/10.1098/rsif.2013.0984>
- [6] V. D. T. Le, A. T. Nguyen, and N. T. Dang, Multibody-dynamics approach to study the deformation and aerodynamics of an insect wing, *AIAA Journal*, vol. 61, no. 6, Mar. 2023, pp. 2500-2516. <https://doi.org/10.2514/1.J061928>
- [7] N. C. Rosenfeld, *An analytical investigation of flappingwing structures for micro air vehicles*, Ph. D, University of Maryland, 2011.
- [8] M. H. Dickinson, F. O. Lehmann, and S. P. Sane, Wing rotation and the aerodynamic basis of insect flight, *Science*, vol. 284, iss. 5422, Jun. 1999, pp. 1954-1960. <https://doi.org/10.1126/science.284.5422.1954>
- [9] N. Phillips and K. Knowles, Effect of flapping kinematics on the mean lift of an insect-like flapping wing, *Proceedings of the Institution of Mechanical Engineers, Part G: Journal of Aerospace Engineering*, vol. 225, iss. 7, Jul. 2011, pp. 723-736. <https://doi.org/10.1177/0954410011401705>
- [10] S. A. Ansari, K. Knowles, and R. Zbikowski, Insectlike flapping wings in the hover part I: Effect of wing kinematics, *Journal of Aircraft*, vol. 45, no. 6, Nov. 2008, pp. 1945-1954. <https://doi.org/10.2514/1.35311>
- [11] T. Nakata, H. Liu, A fluid-structure interaction model of insect flight with flexible wings, *Journal of Computational Physics*, vol. 231, iss.4, Feb. 2012, pp. 1822-1847. <https://doi.org/10.1016/j.jcp.2011.11.005>
- [12] K. B. Lua, X. H. Zhang, T. T. Lim, and K. S. Yeo, Effects of pitching phase angle and amplitude on a two-dimensional flapping wing in hovering mode, *Experiments in Fluids*, vol. 56, Feb. 2015. <https://doi.org/10.1007/s00348-015-1907-9>
- [13] J. Katz and A. Plotkin, *Low-Speed Aerodynamics*, 2nd edi., Cambridge University Press, 2012. <https://doi.org/10.1017/CBO9780511810329>
- [14] D. Tang, S. Bao, B. Lv, H. Guo, L. Luo, and J. Mao, A derivative-free algorithm for nonlinear equations and its applications in multibody dynamics, *Journal of Algorithms & Computational Technology*, vol. 12, iss. 1, Sep. 2017, pp. 30-42. <https://doi.org/10.1177/1748301817729990>
- [15] K. B. Lua, T. T. Lim, and K. S. Yeo, Scaling of aerodynamic forces of three-dimensional flapping wings, *AIAA Journal*, vol. 52, no. 5, May. 2014, pp. 1095-1101. <https://doi.org/10.2514/1.J052730>
- [16] R. P. O'Hara and A. N. Palazotto, The morphological characterization of the forewing of the *Manduca sexta* species for the application of biomimetic flapping wing micro air vehicles, *Bioinspir Biomim*, vol. 7, no. 4, Oct. 2012, pp. 046011. <https://doi.org/10.1088/1748-3182/7/4/046011>
- [17] A. T. Nguyen, J.-K. Kim, J.-S. Han, and J.-H. Han, Extended unsteady vortex-lattice method for insect

- flapping wings, *Journal of Aircraft*, vol. 53, no. 6, Nov. 2016, pp. 1709-1718.
<https://doi.org/10.2514/1.C033456>
- [18] A. P. Willmott and C. P. Ellington, The mechanics of flight in the hawkmoth *manduca sexta*. I. Kinematics of hovering and forward flight, *Journal of Experimental Biology*, vol. 200, iss. 21, Nov. 1997, pp. 2705-2722.
<https://doi.org/10.1242/jeb.200.21.2705>